DFG-Schwerpunktprogramm 1324

„Extraktion quantifizierbarer Information aus komplexen Systemen”

Image Separation Using Shearlets

G. Kutyniok, W.-Q Lim

Preprint 69

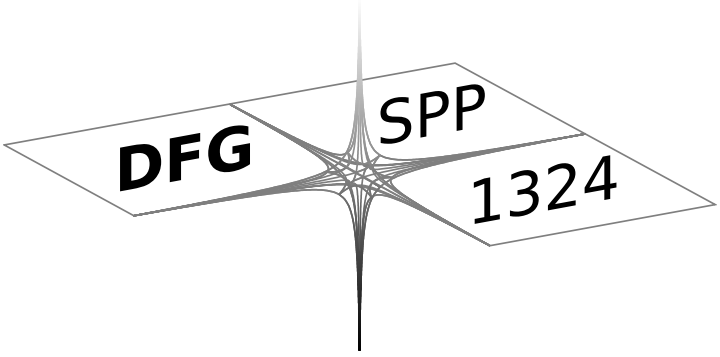

Edited by

AG Numerik/Optimierung
Fachbereich 12 - Mathematik und Informatik
Philipps-Universität Marburg
Hans-Meerwein-Str.
35032 Marburg

DFG-Schwerpunktprogramm 1324

„Extraktion quantifizierbarer Information aus komplexen Systemen”

Image Separation Using Shearlets

G. Kutyniok, W.-Q Lim

Preprint 69

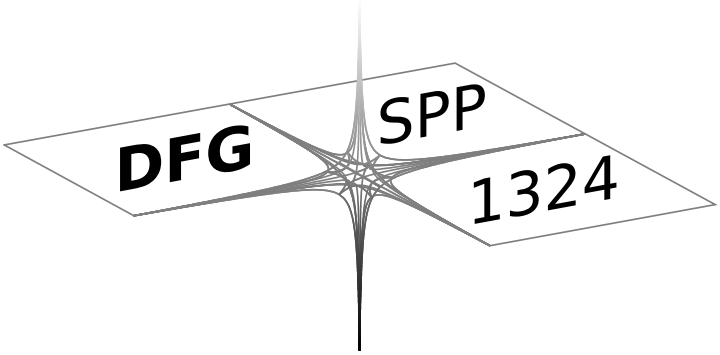

The consecutive numbering of the publications is determined by their chronological order.

The aim of this preprint series is to make new research rapidly available for scientific discussion. Therefore, the responsibility for the contents is solely due to the authors. The publications will be distributed by the authors.

Image Separation Using Shearlets

Gitta Kutyniok and Wang-Q Lim

Institute of Mathematics, University of Osnabrück,
49069 Osnabrück, Germany
kutyniok,wlim@uni-osnabrueck.de

Abstract. In this paper, we present an image separation method for separating images into point- and curvelike parts by employing a combined dictionary consisting of wavelets and shearlets utilizing the fact that they sparsely represent point and curvilinear singularities, respectively. Our methodology is based on the very recently introduced mathematical theory of geometric separation, which shows that highly precise separation of the morphologically distinct features of points and curves can be achieved by ℓ^1 minimization. We further provide and discuss an efficient numerical scheme to solve the associated optimization problem. Finally, we present some experimental results showing the effectiveness of our algorithm.

Keywords: Geometric separation, ℓ_1 minimization, sparse approximation, shearlets, wavelets

1 Introduction

The task of separating an image into its morphologically different contents has recently drawn a lot of attention in the research community due to its significance for applications. In neurobiological imaging, it would, for instance, be desirable to separate 'spines' (pointlike objects) from 'dendrites' (curvelike objects) in order to analyze them independently aiming to detect characteristics of Alzheimer disease. Also, in astronomical imaging, astronomers would often like to separate stars from filaments for further analysis, hence again separating point- from curvelike structures. Successful methodologies for efficiently and accurately solving this task can in fact be applied to a much broader range of areas in science and technology including medical imaging, surveillance, and speech processing.

Although the problem of separating morphologically distinct features seems to be intractable – the problem is underdetermined, since there is only one known data (the image) and two or more unknowns (the images containing the to be extracted features) – experimental results using Morphological Component Analysis [20] suggest that such a separation task might be possible provided that we have prior information about the type of features to be extracted and provided that the morphological difference between those is strong enough. For the separation of point- and curvelike features, it was in fact recently even theoretically

proven in [4] that ℓ_1 minimization solves this task with arbitrarily high precision exploring a combined dictionary of wavelets and curvelets. Wavelets provide optimally sparse expansions for pointlike structures, and curvelets provide optimally sparse expansions for curvelike structures. Thus ℓ_1 minimization applied to the expansion coefficients of the original image into this combined dictionary forces the pointlike structures into the wavelet part and the curvelike structures into the curvelet part, thereby automatically separating the image. An associated algorithmic approach using wavelets and curvelets has been implemented in MCALab[1].

Recently, a novel directional representation system – so-called shearlets – has emerged which provides a unified treatment of continuum models as well as digital models, allowing, for instance, a precise resolution of wavefront sets, optimally sparse representations of cartoon-like images, and associated fast decomposition algorithms; see the survey paper [13]. Shearlet systems are systems generated by one single generator with parabolic scaling, shearing, and translation operators applied to it, in the same way wavelet systems are dyadic scalings and translations of a single function, but including a directionality characteristic owing to the additional shearing operation (and the anisotropic scaling). The shearing operation in fact provides a more favorable treatment of directions, thereby ensuring a unified treatment of the continuum and digital realm as opposed to curvelets which are rotation-based, see [1].

Thus, it is natural to ask whether also a combined dictionary of wavelets and shearlets might be utilizable for separating point- and curvelike features, the advantage presumably being a faster scheme, a more precise separation, and a direct applicability of theoretical results achieved for the continuum domain. And, in fact, the theoretical results from [4] based on a model situation were shown to also hold for a combined dictionary of wavelets and shearlets [3]. Moreover, numerical results give evidence to the superior behavior of shearlet-based decomposition algorithms when compared to curvelet-based algorithms; see [13] for a comparison of ShearLab[2] with CurveLab[3].

In this paper, we will present a novel approach to the separation of point- and curvelike features exploiting a combined dictionary of wavelets and shearlets as well as utilizing block relaxation in a particular way. Numerical results give evidence that indeed the previously anticipated advantages hold true, i.e., that this approach is superior to separation algorithms using wavelets and curvelets such as MCALab in various ways, in particular, our algorithm is faster and provides a more precise separation. In the spirit of reproducible research [5], our algorithm is included in the freely available ShearLab toolbox.

This paper is organized as follows. In Section 2, we introduce the multiscale system of shearlets, and Section 3 reviews the mathematical theory of geometric separation of point- and curvelike features. Our novel algorithmic approach is

[1] MCALab (Version 120) is available from `http://jstarck.free.fr/jstarck/Home.html`.
[2] ShearLab (Version 1.0) is available from `http://www.shearlab.org`.
[3] CurveLab (Version 2.1.2) is available from `http://www.curvelet.org`.

then presented in Section 4 with numerical results discussed in Section 5. We finish the paper with some conclusions.

2 Shearlets

In most multivariate problems, important features of the considered data are concentrated on lower dimensional manifolds. For example, in image processing an edge is an 1D curve that follows a path of rapid change in image intensity. Recently, the novel directional representation system of shearlets [15, 9] has emerged to provide efficient tools for analyzing the intrinsic geometrical features of a signal using anisotropic and directional window functions. In this approach, directionality is achieved by applying integer powers of a shear matrix, and those operations preserve the structure of the integer lattice which is crucial for digital implementations. In fact, this key idea leads to a unified treatment of the continuum as well as digital realm, while still providing optimally sparse approximations of anisotropic features. As already mentioned before, shearlet systems are generated by parabolic scaling, shearing, and translation operators applied to one single generator. Let us now be more precise and formally introduce shearlet systems in 2D.

We first start with some notations and definitions for later use. For $j \geq 0$ and $k \in \mathbb{Z}$, let

$$A_{2^j} = \begin{pmatrix} 2^j & 0 \\ 0 & 2^{\lfloor j/2 \rfloor} \end{pmatrix}, \quad \tilde{A}_{2^j} = \begin{pmatrix} 2^{\lfloor j/2 \rfloor} & 0 \\ 0 & 2^j \end{pmatrix}, \quad \text{and} \quad S_k = \begin{pmatrix} 1 & k \\ 0 & 1 \end{pmatrix}.$$

We can now define so-called cone-adapted discrete shearlet systems, where the term 'cone-adapted' originates from the fact that these systems tile the frequency domain in a cone-like fashion (see Figures 1 and 2). For this, let c be a positive constant, which will later control the sampling density. For $\phi, \psi, \tilde{\psi} \in L^2(\mathbb{R}^2)$, the *cone-adapted discrete shearlet system* $SH(\phi, \psi, \tilde{\psi}; c)$ is then defined by

$$SH(\phi, \psi, \tilde{\psi}; c) = \Phi(\phi; c) \cup \Psi(\psi; c) \cup \tilde{\Psi}(\tilde{\psi}; c),$$

where

$$\Phi(\phi; c) = \{\phi(\cdot - cm) : m \in \mathbb{Z}^2\},$$
$$\Psi(\psi; c) = \{2^{\frac{3}{4}j} \psi(S_k A_{2^j} \cdot - cm) : j \geq 0, -2^{\lceil j/2 \rceil} \leq k \leq 2^{\lceil j/2 \rceil}, m \in \mathbb{Z}^2\},$$

and

$$\tilde{\Psi}(\tilde{\psi}; c) = \{2^{\frac{3}{4}j} \tilde{\psi}(S_k^T \tilde{A}_{2^j} \cdot - cm) : j \geq 0, -2^{\lceil j/2 \rceil} \leq k \leq 2^{\lceil j/2 \rceil}, m \in \mathbb{Z}^2\}.$$

2.1 Band-limited Shearlets

We now first describe the construction of band-limited shearlets which even provide tight frames for $L^2(\mathbb{R}^2)$. The classical example of a generating band-limited shearlet is a function $\psi \in L^2(\mathbb{R}^2)$ satisfying

$$\hat{\psi}(\xi) = \hat{\psi}(\xi_1, \xi_2) = \hat{\psi}_1(\xi_1)\, \hat{\psi}_2(\tfrac{\xi_2}{\xi_1}), \tag{1}$$

where ψ_1 is a band-limited wavelet and $\psi_2 \in L^2(\mathbb{R})$ a scaling function, both satisfying weak decay and smoothness conditions. For more details, we refer the reader to [15, 9].

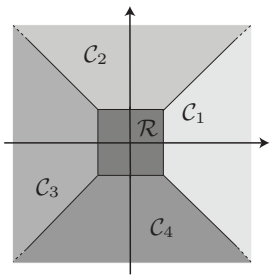

Fig. 1. The cones $\mathcal{C}_1 - \mathcal{C}_4$ and the centered rectangle $\mathcal{R}$ in the frequency domain.

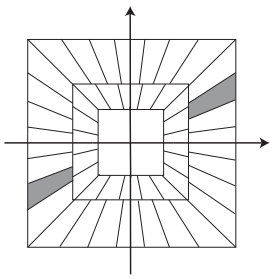

Fig. 2. Tiling of the frequency domain induced by band-limited shearlets.

The tiling of the frequency domain achieved by these band-limited generators while choosing $\tilde{\psi}(x_1, x_2) = \psi(x_2, x_1)$ is illustrated in Figure 2. As described in Figure 1, a conic region $\mathcal{C}_1 \cup \mathcal{C}_3$ is covered by the frequency support of shearlets in $\Psi(\psi; c)$ while $\mathcal{C}_2 \cup \mathcal{C}_4$ is covered by $\tilde{\Psi}(\tilde{\psi}; c)$. For this particular choice, and using an appropriate scaling function ϕ for the centered rectangle $\mathcal{R}$ (see Figure 1), it was proved in [9] that the associated cone-adapted discrete shearlet system $SH(\phi, \psi, \tilde{\psi}; 1)$ forms a tight frame for $L^2(\mathbb{R}^2)$.

2.2 Compactly Supported Shearlets

Although band-limited shearlets might have fast decay in spatial domain, for various applications compact support in spatial domain is highly desirable. In [11], a comprehensive theory introducing and studying compactly supported shearlet systems is provided. One nice feature is that the scaling function $\phi \in L^2(\mathbb{R}^2)$ and the shearlet generators ψ, $\tilde{\psi} \in L^2(\mathbb{R}^2)$ can be chosen to be separable functions, i.e.,

$$\phi(x_1, x_1) = \psi_2(x_1)\psi_2(x_2), \ \psi(x_1, x_2) = \psi_1(x_1)\psi_2(x_2), \text{ and } \tilde{\psi} = \psi(x_2, x_1),$$

where $\psi_1 \in L^2(\mathbb{R})$ can be chosen to be any sufficiently smooth wavelet with enough vanishing moments, at least four, and $\psi_2 \in L^2(\mathbb{R})$ a suitable scaling function. For this type of construction, the separability of the shearlet generator ψ leads to fast digital implementations [16]. The only drawback of this construction is the fact that the associated shearlet systems do not form tight frames for $L^2(\mathbb{R})$. This apparent problem is however attenuated by favorable estimates for the ratio of the associated frame bounds [11]. Finally, we would like to mention that these constructions of 2D shearlets can be extended to 3D for compactly

supported shearlets as well as band-limited shearlets. For more details, we wish to refer the interested reader to [12, 14].

2.3 Optimally Sparse Approximations of Shearlets

Since shearlets are designed to efficiently encode anisotropic features, in particular, curves, one might ask for a precise mathematical formulation of this behavior. As an appropriate model, in [1], Candés and Donoho introduced a special class of 2D functions, called cartoon-like images. *Cartoon-like images* are piecewise smooth 2D functions which are C^2 smooth apart from C^2 singularity curves. They then proved that curvelets provide optimally sparse approximations of elements of this class. Since then, it was shown that also both band-limited shearlets [10] as well as compactly supported shearlets [14] provide the same approximation rate as curvelets, i.e.,

$$\|f - f_N\|_2^2 \leq C \cdot N^{-2} \cdot (\log N)^3 \quad \text{as } N \to \infty,$$

where f is a cartoon-like image and f_N is the nonlinear shearlet approximation obtained by taking the N largest shearlet coefficients in absolute value. This result on optimally sparse approximation has been extended to the 3D situation in [12]. In fact, in [12], sparse approximation properties of shearlets for an even more general class of piecewise smooth functions, namely C^β smooth functions apart from piecewise C^α discontinuities with $1 < \alpha \leq \beta \leq 2$ are discussed.

3 Mathematical Theory of Geometric Separation

In [20], a novel image separation method – Morphological Component Analysis (MCA) – based on sparse representations of images was introduced. In this approach, it is assumed that each image is the linear combination of several components that are morphologically distinct – for instance, points, curves, and textures. The success of this method relies on the assumption that each of the components is sparsely represented in a specific representation system. The key idea is then the following: Provided that such representation systems are identified, the usage of a pursuit algorithm searching for the sparsest representation of the image with respect to the dictionary combining all those specific representation systems will lead to the desired separation.

Various experimental results in [20] show the effectiveness of this method for image separation however without any accompanying mathematical justification. Recently, the first author of this paper and Donoho developed a mathematical framework in [4] within which the notion of successful separation can be made definitionally precise and can be mathematically proven in case of separating point- from curvelike features, which they coined *Geometric Separation*. One key ingredient of their analysis is the consideration of clustered sparsity properties measured by so-called *cluster coherence*. In this section, we briefly review this theoretical approach to the Geometric Separation Problem, which will serve as the foundation for our algorithm.

3.1 Model Situation

As a mathematical model for a composition of point- and curvelike structures, we consider the following two components: As a 'point-like' object, we consider the function $\mathcal{P}$ which is smooth except for point singularities and is defined by

$$\mathcal{P} = \sum_{i=1}^{P} |x - x_i|^{-3/2}.$$

As a 'curve-like' object, we consider the distribution $\mathcal{C}$ with singularity along a closed curve $\tau : [0, 1] \to \mathbb{R}^2$ defined by

$$\mathcal{C} = \int \delta_{\tau(t)} dt.$$

Then our model situation is the sum of both, i.e.,

$$f = \mathcal{P} + \mathcal{C}. \tag{2}$$

The Geometric Separation Problem now consists of recovering $\mathcal{P}$ and $\mathcal{C}$ from the observed signal f.

3.2 Chosen Dictionary

As we indicated before, it is now crucial to choose two representations systems each of which sparsely represents one of the morphologically different components in the Geometric Separation Problem. Our sparse approximation result, described in the previous section, suggests that curvilinear singularities can be sparsely represented by shearlets. On the other hand, it is well known that wavelets can provide optimally sparse approximations of functions which are smooth apart from point singularities. Hence, we choose the overcomplete system within which we will expand the signal f as a composition of the following two systems:

- *Orthonormal Separable Meyer Wavelets*: Band-limited wavelets which form an orthonormal basis of isotropic generating elements.
- *Bandlimited Shearlets*: A directional and anisotropic tight frame generated by a band-limited shearlet generator ψ defined in Section 2.

3.3 Subband Filtering

Since the scaling subbands of shearlets and wavelets are similar as illustrated in Figures 2 and 3, we can define a family of filters $(F_j)_j$ which allows to decompose a function f into pieces f_j with different scales j depending on those subbands. The piece f_j associated to subband j arises from filtering f using F_j by

$$f_j = F_j * f,$$

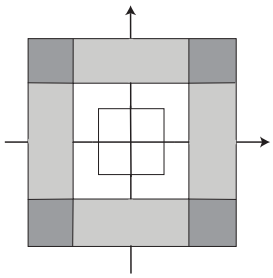

Fig. 3. Tiling of the frequency domain induced by wavelets.

resulting in a function whose Fourier transform $\hat{f}_j$ is supported on the scaling subband of scale j of the wavelet as well as the shearlet frame. The filters are defined in such way, that the original function can be reconstructed from the sequence $(f_j)_j$ using

$$f = \sum_j F_j * f_j, \quad f \in L^2(\mathbb{R}^2).$$

We can now exploit these tools to attack the Geometric Separation Problem scale-by-scale. For this, we filter the model problem (2) to derive the sequence of filtered images

$$f_j = \mathcal{P}_j + \mathcal{C}_j \quad \text{for all scales } j.$$

3.4 ℓ_1 Minimization Problem

Let now Φ_1 and Φ_2 be an orthonormal basis of band-limited wavelets and a tight frame of band-limited shearlets, respectively. Then, for each scale j, we consider the following optimization problem:

$$(\hat{W}_j, \hat{S}_j) = \text{argmin}_{W_j, S_j} \|\Phi_1^T W_j\|_1 + \|\Phi_2^T S_j\|_1 \quad \text{subject to} \quad f_j = W_j + S_j. \quad (3)$$

Notice that $\Phi_1^T W_j$ and $\Phi_2^T S_j$ are the wavelet and shearlet coefficients of the signals W_j and S_j, respectively. We wish to further remark, that here the ℓ_1 norm is placed on the analysis rather than the synthesis coefficients to avoid numerical instabilities due to the redundancy of the shearlet frame.

3.5 Theoretical Result

The theoretical result of the precision of separation of f_j via (3) proved in [4] and [3] can now be stated in the following way:

Theorem 1 ([4] and [3]). *Let $\hat{W}_j$ and $\hat{S}_j$ be the solutions to the optimization problem (3) for each scale j. Then we have*

$$\frac{\|\mathcal{P}_j - \hat{W}_j\|_2 + \|\mathcal{C}_j - \hat{S}_j\|_2}{\|\mathcal{P}_j\|_2 + \|\mathcal{C}_j\|_2} \to 0, \quad j \to \infty.$$

This result shows that the components $\mathcal{P}_j$ and $\mathcal{C}_j$ are recovered with asymptotically arbitrarily high precision at very fine scales. The energy in the pointlike component is completely captured by the wavelet coefficients, and the curvelike component is completely contained in the shearlet coefficients. Thus, the theory evidences that the Geometric Separation Problem can be satisfactorily solved by using a combined dictionary of wavelets and shearlets and an appropriate ℓ_1 minimization problem.

4 Our Algorithmic Approach to the Geometric Separation Problem

In this section, we present our algorithmic approach to the Geometric Separation Problem of separating point- from curvelike features by using a combined dictionary of wavelets and shearlets. The ingredients of the algorithm we be detailed below.

4.1 General Scheme

In practice, the observed signal f is often contaminated by noise which requires an adaption of the optimization problem (3). As proposed in numerous publications, one typically considers a modified optimization problem – so-called Basis Pursuit Denoising (BPDN) – which can be obtained by relaxing the constraint in (3) in order to deal with noisy observed signals (see [19]). For each scale j, the optimization problem then takes the form:

$$(\hat{W}_j, \hat{S}_j) = \text{argmin}_{W_j, S_j} \|\Phi_1^T W_j\|_1 + \|\Phi_2^T S_j\|_1 + \lambda \|f_j - W_j - S_j\|_2^2. \quad (4)$$

In this new form, the additional content in the image – the noise – characterized by the property that it can not be represented sparsely by either one of the two representation systems will be allocated to the residual $f_j - W_j - S_j$. Hence, performing this minimization, we not only separate point- and curvelike objects, which were modeled by $\mathcal{P}_j$ and $\mathcal{C}_j$ in Subsection 3.1, but also succeed in removing an additive noise component as a by-product. Of course, solving the optimization problem (4) for all relevant scales j is computationally expensive.

4.2 Preprocessing

To avoid high complexity, we observe that the frequency distribution of point- and curvelike components is highly concentrated on high frequencies. Hence it would be essentially sufficient for achieving accurate separation to solve (4) for only sufficiently large scales j, as also evidenced by Theorem 1. This idea leads to a simplification of the problem (4) by modifying the observed signal f as follows: We first consider bandpass filters $F_0, \ldots, F_L$, where $(F_j)_{j=0,\ldots,L}$ is the

family of bandpass filters defined in Subsection 3.3 up to scale L, and F_0 is a lowpass filter. Thus the observed signal f satisfies

$$f = \sum_{j=0}^{L} F_j * f_j \quad \text{with } f_j = F_j * f.$$

For each scale j, we now carefully choose a non-uniform weight $w_j > 0$ satisfying, in particular, $w_j < w_{j'}$, if $j < j'$. These weights are then utilized for a weighted reconstruction of f resulting in a newly constructed signal $\tilde{f}$ by computing

$$\tilde{f} = \sum_{j=0}^{L} w_j \cdot (F_j * f_j). \tag{5}$$

In this way, the two morphological components, namely points and curves, can be enhanced by suppressing the low frequencies.

4.3 Solver for the ℓ_1 Minimization Problem

Using the reweighted reconstruction of f from (5) coined $\tilde{f}$, we now consider the following new minimization problem:

$$(\hat{W}, \hat{S}) = \text{argmin}_{W,S} \|\Phi_1^T W\|_1 + \|\Phi_2^T S\|_1 + \lambda \|\tilde{f} - W - S\|_2^2. \tag{6}$$

Note that the frequency distribution of $\tilde{f}$ is highly concentrated on the high frequencies – in other words, scaling subbands of large scales j –, and Theorem 1 justifies our expectation of a very precise separation using $\tilde{f}$ instead of f. Even more advantageous, the reduced problem (6) no longer involves different scales j, and hence can be efficiently solved by various fast numerical schemes. In our algorithm, we choose the Block Coordinate Relaxation (BCR) method from [18].

To briefly review the BCR method, let us consider the following optimization problem:

$$\hat{\alpha} = \text{argmin}_{\alpha} \|\alpha\|_1 + \lambda \|s - \Phi\alpha\|_2^2, \tag{7}$$

where α and s are column vectors in $\mathbb{R}^{NL}$ and $\mathbb{R}^N$, respectively, and λ is some positive constant. Further, we assume that Φ is an $N \times LN$-matrix consisting of L orthonormal bases Φ_i for $\mathbb{R}^N$. That is, we have $\Phi = [\Phi_1, \ldots, \Phi_{LN}]$ so that the column vectors of each submatrix Φ_i form an orthonormal basis for $\mathbb{R}^N$. If $L = 1$, the matrix Φ becomes orthonormal in which case the problem (7) has the following closed form solution:

$$\hat{\alpha} = \eta_\lambda(\Phi^T s), \tag{8}$$

where η_λ is applied coordinatewise to the vector $\Phi^T s$. The function η_λ is known as the soft shrinkage function and is defined by:

$$\eta_\lambda(x) = \frac{x}{|x|}(|x| - 2/\lambda)_+.$$

This closed form solution forms the core of the BCR method for solving (7), which performs the following steps: We start by making an initial guess $\alpha_0 \in \mathbb{R}^{NL}$, and selecting an index $i_1 \in \{1, \dots, L\}$ such that the correlations between specific successive submatrices are minimized. For more details about this selection process, we refer to [18]. The next vector α_1 is then computed in the following way, which for brevity purposes we detail assuming we are already in the m-th step. We first partition the vector α_{m-1} and the columns of Φ into two sets: $\alpha_{m-1}^{(i_m)}$ corresponding to the columns in the submatrix Φ_{i_m} and $\alpha_{m-1}^{(-i_m)}$ corresponding to the remaining columns Φ_{-i_m}. Defining the residual vector $v^{(m)}$ by

$$v^{(m)} = s - \Phi_{-i_m} \alpha_{m-1}^{(-i_m)},$$

we obtain the subproblem

$$\alpha_m^{(i_m)} = \operatorname{argmin}_{\alpha \in \mathbb{R}^N} \|\alpha\|_1 + \lambda \|v^{(m)} - \Phi_{i_m} \alpha\|_2^2. \tag{9}$$

Since the submatrix Φ_{i_m} is orthonormal, this problem can be solved by (8) and results in the updating of the entries in the i_m-th block of the vector α_m in each m-th iteration step. These steps are now repeated for $m = 1, 2, \dots$ until a preselected convergence criterion is met.

One main advantage of the BCR method is that each iteration step described in (9) only requires matrix multiplication with a unitary matrix. Furthermore, it is not necessary to keep the full matrix Φ in memory. This is particularly important when redundant transforms associated with the matrix Φ are used, which is exactly our situation.

After this presentation of the general form of BCR, let us now focus on the situation at hand. For this, we assume that $L = 2$ and $\Phi = [\Phi_1, \Phi_2]$, where the column vectors in each of the submatrix Φ_i form a tight frame for $\mathbb{R}^N$, i.e.,

$$\Phi_i \Phi_i^T = I_N \quad \text{for } i = 1, 2,$$

where I_N is an $N \times N$ identity matrix. Then the problem (7) becomes

$$\begin{aligned} (\hat{\beta}_1, \hat{\beta}_2) = \operatorname{argmin}_{(\beta_1, \beta_2, r_1, r_2)} & \|\Phi_1^T \beta_1 + r_1\|_1 + \|\Phi_2^T \beta_2 + r_2\|_1 + \lambda \|s - \beta_1 - \beta_2\|_2^2 \\ & \text{subject to } \Phi_1 r_1 = 0,\ \Phi_2 r_2 = 0. \end{aligned} \tag{10}$$

Notice that, for each $i = 1, 2$, Φ_i^T is an overcomplete linear transform applied to the vector $\beta_i \in \mathbb{R}^N$. If we now choose $r_1 = r_2 = 0$, the minimization problem (10) coincides with the minimization problem (6) with $s = \tilde{f}, W = \beta_1$, and $S = \beta_2$. Thus, (6) can be solved by the BCR method we described above; and only some very minor changes due to the non-unitarity of the transforms now involved are required, see [20].

In the following subsections, we discuss the particular form of the matrices Φ_1^T and Φ_2^T which encode the wavelet and shearlet transform in the minimization problem (6) we aim to solve.

4.4 Wavelet Transform

Let us start with the wavelet transform. The undecimated digital wavelet transform is certainly the most fitting version of the wavelet transform for the filtering of data, and hence this is what we utilize also here. This transform is obtained by skipping the subsampling, thereby yielding an overcomplete transform, which in addition is shift-invariant. The redundancy factor of this transform is $3J + 1$, where J is the number of decomposition levels. We refrain from further details and merely refer the reader to [17].

4.5 Shearlet Transform

For the shearlet transform, we employ the digital shearlet transform implemented by 2D convolution with discretized band-limited shearlets, which was first introduced in [6]. This implementation shows that the directional selectivity of shearlets can be faithfully adapted to the digital setting, since the action of shearing providing the directionality of shearlets preserves the structure of the integer lattice $\mathbb{Z}^2$. This allows highly precise extraction of directional features, e.g., edges, from digitalized images, which is in fact crucial for extracting curve-like components. Let us finally mention that for image separation, band-limited shearlets are superior to compactly supported shearlets, since they provide a tight frame as well as excellent directional selectivity due to their high localization in the frequency domain.

To describe this digital shearlet transform in more detail, let $F_0, \dots, F_L$ be the band-pass filters introduced in Subsection 3.3 up to scale L, where F_0 is a low-pass filter. We now let $\tilde{F}_0, \dots, \tilde{F}_L$ be dual filters such that the following reconstruction formula holds:

$$f = \sum_{j=0}^{L} \tilde{F}_j * (F_j * f) \qquad \text{for } f \in \ell^2(\mathbb{Z}^2). \tag{11}$$

Next, we carefully select a frequency-based window function W such that

$$\sum_{k=-2^{\lceil j/2 \rceil}}^{2^{\lceil j/2 \rceil}} W[2^{\lceil j/2 \rceil} n_2 - k] = 1.$$

Denoting a chosen mapping function from the Cartesian grid to the pseudo-polar grid by φ_P, for each $j > 0$ and k, we define the discrete Fourier transform of directional filters $w_{j,k}$ by

$$\hat{w}_{j,k}[n_1, n_2] = \varphi_P^{-1}(\hat{\delta}_P[n_1, n_2] W[2^{\lceil j/2 \rceil} n_2 - k]),$$

where $\hat{\delta}_P$ represents the discrete Fourier transform of the delta function on the pseudo-polar grid. We now assume that φ_P was chosen such that

$$\sum_{k=-2^{\lceil j/2 \rceil}}^{2^{\lceil j/2 \rceil}} \hat{w}_{j,k}[n_1, n_2] = 1, \tag{12}$$

which is possible, and we would like to refer to [2] for more details. Finally, for $f \in \ell^2(\mathbb{Z}^2)$, we define the *digital shearlet transform* $SH_\psi : f \to SH_\psi f(j,k,n)$ by

$$SH_\psi f(j,k,n) = (f * \psi_{j,k})[n_1, n_2],$$

where $n = (n_1, n_2) \in \mathbb{Z}^2$ and $\psi_{j,k}$ are the discretized shearlets defined by

$$\psi_{j,k}[n_1, n_2] = (F_j * w_{j,k})[n_1, n_2].$$

Figure 4 shows the magnitude response of some so-called shearlet filters, which is defined by the absolute values of the trigonometric polynomial whose Fourier coefficients are $\psi_{j,k}[n_1, n_2]$.

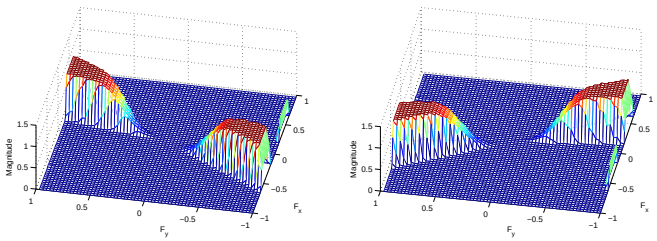

Fig. 4. Magnitude response of the shearlet filters at the finest scale.

By (11) and (12), we then have the following reconstruction formula:

$$f = \tilde{F}_0 * (F_0 * f) + \sum_{j=1}^{L} \sum_{k=-2^{\lceil j/2 \rceil}}^{2^{\lceil j/2 \rceil}} \tilde{F}_j * (\psi_{j,k} * f),$$

thus an inverse transform.

We wish to remark that the digital shearlet transform we described above is shift-invariant. Furthermore, it can be efficiently implemented by using the FFTW algorithm from [8], which implements fast 2D convolution via FFT in particular way, to improve the complexity of this digital shearlet transform and its inverse.

5 Numerical Results

In this section, we present and discuss some numerical results of our proposed scheme for separating point- and curvelike features. In each experiment we compare our scheme, which is freely available in the ShearLab[4] toolbox, with the separation algorithm MCALab[5]. In contrast to our algorithm, MCALab uses wavelets and curvelets to separate point- and curvelike components, and we refer to [7] for more details on the algorithm.

[4] ShearLab (Version 1.0) is available from `http://www.shearlab.org`.

[5] MCALab (Version 120) is available from `http://jstarck.free.fr/jstarck/Home.html`.

5.1 Discussion of Figure 5

Figure 5a is an artificial image consisting of a composition of point- and curvelike structures on a smooth background, and Figure 5b is the same image with some additive white Gaussian noise. The comparison of Figures 5c and 5d shows that while extracting pointlike structures, MCALab still keeps some of the curvelike content. In contrast to this, the only visible artifacts our scheme produces are at the intersections of the curvelike structures, for which it is even justified to label them as 'points'. It also becomes evident, that MCALab has problems with the smooth background which is also partially extracted. Next, comparing Figures 5e and 5f, the difference between both algorithms is not that strong. However, visible evidence still attests a cleaner extraction of the curvelike part by our scheme. Finally, the comparison of the computing time shows that the separation can be much faster performed by our scheme, which deserves a careful discussion which along the way will also lead to a better understanding of the differences between our scheme and MACLab.

As detailed in Section 2, shearlet systems use regular translations on the integer lattice as well as shearing operations providing directionality while preserving the structure of the integer grid. These two properties naturally lead to an implementation of the digital shearlet transform exploiting discrete convolutions, which allows us to obtain a shift-invariant transform by simply skipping the anisotropic downsampling similar to the wavelet case. Therefore, the resulting digital shearlet transform is highly redundant when compared to the digital curvelet transform in CurveLab[6]. However, although the curvelet transform is less redundant and faster than the considered shift-invariant digital shearlet transform, the property of shift-invariance bought with this additional redundancy provides a much more accurate extraction of curvelike features. Carefully analyzing Figures 5e and 5f, we see that curvelets do a relatively good job when capturing lines, since these simple objects can be well represented by only a few curvelet elements. However, the curvelet transform performs poorly for curved singularities like the circle, since these objects are highly complex and much more curvelet elements are needed to capture them. In fact, this is the point at which the redundancy of the considered digital shearlet transform comes into play, since this transform provides 'enough' shearlet elements to accurately represent a complex object like a circle. An additional aspect to be considered is the fact that this digital shearlet transform is very easy to implement, its main ingredient being 2D fast convolution.

It seems though a little surprising that our separation scheme is still faster than MCALab. The reason is firstly the efficient implementation of the digital shearlet transform and secondly the fact that the shift-invariance bought by additional redundancy provides a much more accurate extraction of curvelike features, which both result in significantly less iterations required by our separation scheme.

[6] CurveLab (Version 2.1.2) is available from `http://www.curvelet.org`.

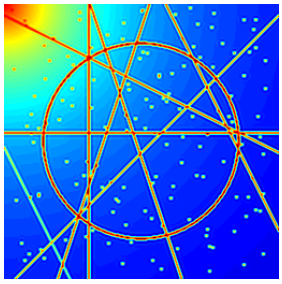

(a) Original image (256×256)

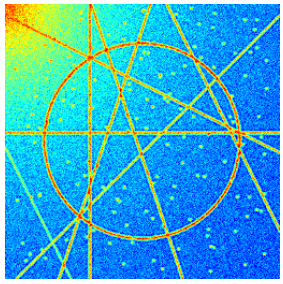

(b) Noisy image

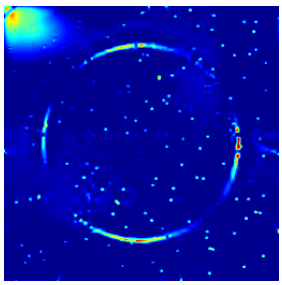

(c) Pointlike Component (MCALab)

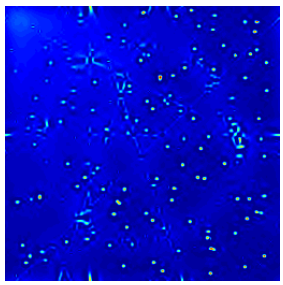

(d) Pointlike Component (Our Scheme)

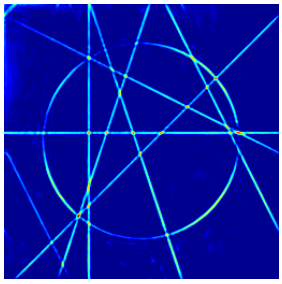

(e) Curvelike Component (MCALab)

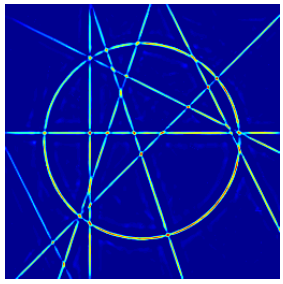

(f) Curvelike Component (Our Scheme)

Fig. 5. Comparison results between MCALab and our scheme for an artificial image. Computing time: 42.74sec (MCALab) and 33.75sec (our scheme).

5.2 Discussion of Figure 6

Let us now consider the performance of our scheme and MCALab on real-world images. Figure 6a is an image of a neuron generated by fluorescence microscopy,

which is composed of 'spines' (pointlike features) and 'dendrites' (curvelike features). Typically, neurobiologists would like to extract those components for further analysis. Comparing Figures 6b and 6c, we see that our scheme extracts the pointlike structures much more precise than MCALab. But the most striking difference appears in the extraction of the curvelike part, where the image generated by MCALab (Figure 6d) contains much thicker footprints of the dendrites than in the original image in Figure 6a. Here, again, our scheme produces a much more precise extraction of the curvelike features. As before, a comparison of the computing time votes in favor of our scheme.

6 Conclusion

In this paper, we introduced a novel methodology for separating images into point- and curvelike features based on the new paradigm of sparse approximation and using ℓ_1 minimization. In contrast to other approaches, our algorithm utilizes a combined dictionary consisting of wavelets and shearlets, implemented as shift-invariant transforms, and is based on a precise mathematical theory. Numerical results show that our scheme extracts point- and curvelike features much more precise and uses less computing time than the state-of-the-art algorithm MCALab, which is based on wavelets and curvelets.

Acknowledgement

The first author would like to thank David Donoho and Michael Elad for inspiring discussions on related topics. We are also grateful to the research group by Roland Brandt for supplying the test image in Figure 6a. The authors acknowledge support from DFG Grant SPP-1324, KU 1446/13. The first author also acknowledges partial support from DFG Grant KU 1446/14.

References

1. E. J. Candés and D. L. Donoho, *New tight frames of curvelets and optimal representations of objects with piecewise C^2 singularities*, Comm. Pure and Appl. Math. **56** (2004), 216–266.
2. F. Colonna and G. R. Easley, *Generalized discrete radon transform and their use in the ridgelet transform*, J. Math. Imaging Vision **23** (2005), 145–165.
3. D. L. Donoho and G. Kutyniok, *Geometric Separation using a Wavelet-Shearlet Dictionary*, SampTA'09 (Marseille, France, 2009), Proc., 2009.
4. D. L. Donoho and G. Kutyniok, *Microlocal analysis of the geometric separation problem*, preprint.
5. D. L. Donoho, A. Maleki, M. Shahram, V. Stodden, and I. Ur-Rahman, *Fifteen years of reproducible research in computational harmonic analysis*, Comput. Sci. Engrg. **11** (2009), 8–18.
6. G. Easley, D. Labate, and W.-Q Lim, *Sparse directional image representations using the discrete shearlet transform*, Appl. Comput. Harmon. Anal. **25** (2008), 25–46.

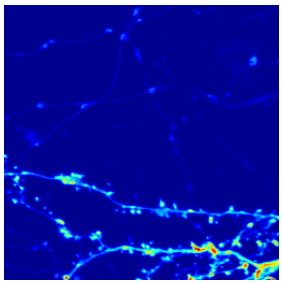

(a) Original image (256×256)

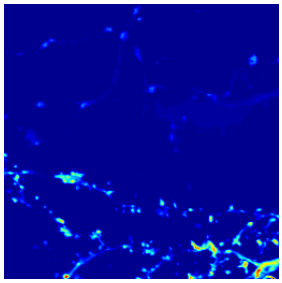

(b) Pointlike Component (MCALab)

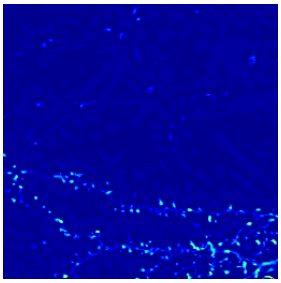

(c) Pointlike Component (Our Scheme)

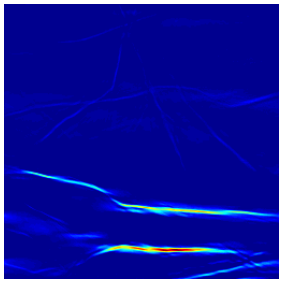

(d) Curvelike Component (MCALab)

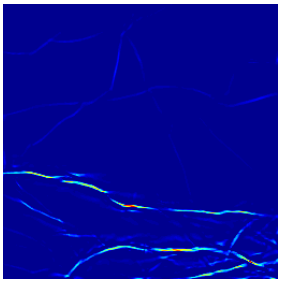

(e) Curvelike Component (Our Scheme)

Fig. 6. Comparison results between MCALab and our scheme for a neuron image. Computing time: 42.74sec (MCALab) and 33.75sec (our scheme).

7. M.J. Fadilli, J.-L Starck, M. Elad, and D. L. Donoho, *MCALab: reproducible research in signal and image decomposition and inpainting*, IEEE Comput. Sci. Eng. Mag., 2009, to appear.
8. M. Frigo and S. G. Johnson, *The design and implementation of FFTW3*, Proc. IEEE **93** (2005), 216–231.

9. K. Guo, G. Kutyniok, and D. Labate, *Sparse multidimensional representations using anisotropic dilation and shear operators*, Wavelets and Splines (Athens, GA, 2005), Nashboro Press, Nashville, TN, 2006, 189–201.
10. K. Guo and D. Labate, *Optimally sparse multidimensional representation using shearlets*, SIAM J. Math Anal. **39** (2007), 298–318.
11. P. Kittipoom, G. Kutyniok, and W.-Q Lim, *Construction of compactly supported shearlet frames*, preprint.
12. G. Kutyniok, J. Lemvig, and W.-Q Lim, *Compactly supported shearlet frames and optimally sparse approximations of functions in $L^2(\mathbb{R}^3)$ with piecewise C^2 singularities*, preprint.
13. G. Kutyniok, J. Lemvig, and W.-Q Lim, *Compactly Supported Shearlets*, Approximation Theory XIII (San Antonio, TX, 2010), Springer, to appear.
14. G. Kutyniok and W.-Q Lim, *Compactly supported shearlets are optimally sparse*, preprint.
15. D. Labate, W.-Q Lim, G. Kutyniok, and G. Weiss. *Sparse multidimensional representation using shearlets*, in Wavelets XI, edited by M. Papadakis, A. F. Laine, and M. A. Unser, SPIE Proc., **5914**, SPIE, Bellingham, WA, 2005, 254–262,
16. W.-Q Lim, *The discrete shearlet transform: A new directional transform and compactly supported shearlet frames*, IEEE Trans. Image Proc. **19** (2010), 1166–1180.
17. S. Mallat, *A wavelet tour of signal processing*, Academic Press, Inc., San Diego, CA, 1998.
18. S. Sardy, A. G. Bruce, and P. Tseng, *Block coordinate relaxation methods for nonparametric signal denoising with wavelet dictionaries*, J. Comput. Graph. Statist. **9** (2000), 361–379.
19. S. S. Chen, D. L. Donoho, and M. A. Saunders, *Atomic decomposition by basis pursuit*, SIAM J. Sci. Comput. **20** (1998), 33–61.
20. J.-L Starck, M. Elad, and D. Donoho, *Image decomposition via the combination of sparse representation and a variational approach*, IEEE Trans. Image Proc. **14** (2005), 1570–1582.

Preprint Series DFG-SPP 1324

http://www.dfg-spp1324.de

Reports

[1] R. Ramlau, G. Teschke, and M. Zhariy. A Compressive Landweber Iteration for Solving Ill-Posed Inverse Problems. Preprint 1, DFG-SPP 1324, September 2008.

[2] G. Plonka. The Easy Path Wavelet Transform: A New Adaptive Wavelet Transform for Sparse Representation of Two-dimensional Data. Preprint 2, DFG-SPP 1324, September 2008.

[3] E. Novak and H. Woźniakowski. Optimal Order of Convergence and (In-) Tractability of Multivariate Approximation of Smooth Functions. Preprint 3, DFG-SPP 1324, October 2008.

[4] M. Espig, L. Grasedyck, and W. Hackbusch. Black Box Low Tensor Rank Approximation Using Fibre-Crosses. Preprint 4, DFG-SPP 1324, October 2008.

[5] T. Bonesky, S. Dahlke, P. Maass, and T. Raasch. Adaptive Wavelet Methods and Sparsity Reconstruction for Inverse Heat Conduction Problems. Preprint 5, DFG-SPP 1324, January 2009.

[6] E. Novak and H. Woźniakowski. Approximation of Infinitely Differentiable Multivariate Functions Is Intractable. Preprint 6, DFG-SPP 1324, January 2009.

[7] J. Ma and G. Plonka. A Review of Curvelets and Recent Applications. Preprint 7, DFG-SPP 1324, February 2009.

[8] L. Denis, D. A. Lorenz, and D. Trede. Greedy Solution of Ill-Posed Problems: Error Bounds and Exact Inversion. Preprint 8, DFG-SPP 1324, April 2009.

[9] U. Friedrich. A Two Parameter Generalization of Lions' Nonoverlapping Domain Decomposition Method for Linear Elliptic PDEs. Preprint 9, DFG-SPP 1324, April 2009.

[10] K. Bredies and D. A. Lorenz. Minimization of Non-smooth, Non-convex Functionals by Iterative Thresholding. Preprint 10, DFG-SPP 1324, April 2009.

[11] K. Bredies and D. A. Lorenz. Regularization with Non-convex Separable Constraints. Preprint 11, DFG-SPP 1324, April 2009.

[12] M. Döhler, S. Kunis, and D. Potts. Nonequispaced Hyperbolic Cross Fast Fourier Transform. Preprint 12, DFG-SPP 1324, April 2009.

[13] C. Bender. Dual Pricing of Multi-Exercise Options under Volume Constraints. Preprint 13, DFG-SPP 1324, April 2009.

[14] T. Müller-Gronbach and K. Ritter. Variable Subspace Sampling and Multi-level Algorithms. Preprint 14, DFG-SPP 1324, May 2009.

[15] G. Plonka, S. Tenorth, and A. Iske. Optimally Sparse Image Representation by the Easy Path Wavelet Transform. Preprint 15, DFG-SPP 1324, May 2009.

[16] S. Dahlke, E. Novak, and W. Sickel. Optimal Approximation of Elliptic Problems by Linear and Nonlinear Mappings IV: Errors in L_2 and Other Norms. Preprint 16, DFG-SPP 1324, June 2009.

[17] B. Jin, T. Khan, P. Maass, and M. Pidcock. Function Spaces and Optimal Currents in Impedance Tomography. Preprint 17, DFG-SPP 1324, June 2009.

[18] G. Plonka and J. Ma. Curvelet-Wavelet Regularized Split Bregman Iteration for Compressed Sensing. Preprint 18, DFG-SPP 1324, June 2009.

[19] G. Teschke and C. Borries. Accelerated Projected Steepest Descent Method for Nonlinear Inverse Problems with Sparsity Constraints. Preprint 19, DFG-SPP 1324, July 2009.

[20] L. Grasedyck. Hierarchical Singular Value Decomposition of Tensors. Preprint 20, DFG-SPP 1324, July 2009.

[21] D. Rudolf. Error Bounds for Computing the Expectation by Markov Chain Monte Carlo. Preprint 21, DFG-SPP 1324, July 2009.

[22] M. Hansen and W. Sickel. Best m-term Approximation and Lizorkin-Triebel Spaces. Preprint 22, DFG-SPP 1324, August 2009.

[23] F.J. Hickernell, T. Müller-Gronbach, B. Niu, and K. Ritter. Multi-level Monte Carlo Algorithms for Infinite-dimensional Integration on $\mathbb{R}^{\mathbb{N}}$. Preprint 23, DFG-SPP 1324, August 2009.

[24] S. Dereich and F. Heidenreich. A Multilevel Monte Carlo Algorithm for Lévy Driven Stochastic Differential Equations. Preprint 24, DFG-SPP 1324, August 2009.

[25] S. Dahlke, M. Fornasier, and T. Raasch. Multilevel Preconditioning for Adaptive Sparse Optimization. Preprint 25, DFG-SPP 1324, August 2009.

[26] S. Dereich. Multilevel Monte Carlo Algorithms for Lévy-driven SDEs with Gaussian Correction. Preprint 26, DFG-SPP 1324, August 2009.

[27] G. Plonka, S. Tenorth, and D. Roşca. A New Hybrid Method for Image Approximation using the Easy Path Wavelet Transform. Preprint 27, DFG-SPP 1324, October 2009.

[28] O. Koch and C. Lubich. Dynamical Low-rank Approximation of Tensors. Preprint 28, DFG-SPP 1324, November 2009.

[29] E. Faou, V. Gradinaru, and C. Lubich. Computing Semi-classical Quantum Dynamics with Hagedorn Wavepackets. Preprint 29, DFG-SPP 1324, November 2009.

[30] D. Conte and C. Lubich. An Error Analysis of the Multi-configuration Time-dependent Hartree Method of Quantum Dynamics. Preprint 30, DFG-SPP 1324, November 2009.

[31] C. E. Powell and E. Ullmann. Preconditioning Stochastic Galerkin Saddle Point Problems. Preprint 31, DFG-SPP 1324, November 2009.

[32] O. G. Ernst and E. Ullmann. Stochastic Galerkin Matrices. Preprint 32, DFG-SPP 1324, November 2009.

[33] F. Lindner and R. L. Schilling. Weak Order for the Discretization of the Stochastic Heat Equation Driven by Impulsive Noise. Preprint 33, DFG-SPP 1324, November 2009.

[34] L. Kämmerer and S. Kunis. On the Stability of the Hyperbolic Cross Discrete Fourier Transform. Preprint 34, DFG-SPP 1324, December 2009.

[35] P. Cerejeiras, M. Ferreira, U. Kähler, and G. Teschke. Inversion of the noisy Radon transform on $SO(3)$ by Gabor frames and sparse recovery principles. Preprint 35, DFG-SPP 1324, January 2010.

[36] T. Jahnke and T. Udrescu. Solving Chemical Master Equations by Adaptive Wavelet Compression. Preprint 36, DFG-SPP 1324, January 2010.

[37] P. Kittipoom, G. Kutyniok, and W.-Q Lim. Irregular Shearlet Frames: Geometry and Approximation Properties. Preprint 37, DFG-SPP 1324, February 2010.

[38] G. Kutyniok and W.-Q Lim. Compactly Supported Shearlets are Optimally Sparse. Preprint 38, DFG-SPP 1324, February 2010.

[39] M. Hansen and W. Sickel. Best m-Term Approximation and Tensor Products of Sobolev and Besov Spaces – the Case of Non-compact Embeddings. Preprint 39, DFG-SPP 1324, March 2010.

[40] B. Niu, F.J. Hickernell, T. Müller-Gronbach, and K. Ritter. Deterministic Multi-level Algorithms for Infinite-dimensional Integration on $\mathbb{R}^{\mathbb{N}}$. Preprint 40, DFG-SPP 1324, March 2010.

[41] P. Kittipoom, G. Kutyniok, and W.-Q Lim. Construction of Compactly Supported Shearlet Frames. Preprint 41, DFG-SPP 1324, March 2010.

[42] C. Bender and J. Steiner. Error Criteria for Numerical Solutions of Backward SDEs. Preprint 42, DFG-SPP 1324, April 2010.

[43] L. Grasedyck. Polynomial Approximation in Hierarchical Tucker Format by Vector-Tensorization. Preprint 43, DFG-SPP 1324, April 2010.

[44] M. Hansen und W. Sickel. Best m-Term Approximation and Sobolev-Besov Spaces of Dominating Mixed Smoothness - the Case of Compact Embeddings. Preprint 44, DFG-SPP 1324, April 2010.

[45] P. Binev, W. Dahmen, and P. Lamby. Fast High-Dimensional Approximation with Sparse Occupancy Trees. Preprint 45, DFG-SPP 1324, May 2010.

[46] J. Ballani and L. Grasedyck. A Projection Method to Solve Linear Systems in Tensor Format. Preprint 46, DFG-SPP 1324, May 2010.

[47] P. Binev, A. Cohen, W. Dahmen, R. DeVore, G. Petrova, and P. Wojtaszczyk. Convergence Rates for Greedy Algorithms in Reduced Basis Methods. Preprint 47, DFG-SPP 1324, May 2010.

[48] S. Kestler and K. Urban. Adaptive Wavelet Methods on Unbounded Domains. Preprint 48, DFG-SPP 1324, June 2010.

[49] H. Yserentant. The Mixed Regularity of Electronic Wave Functions Multiplied by Explicit Correlation Factors. Preprint 49, DFG-SPP 1324, June 2010.

[50] H. Yserentant. On the Complexity of the Electronic Schrödinger Equation. Preprint 50, DFG-SPP 1324, June 2010.

[51] M. Guillemard and A. Iske. Curvature Analysis of Frequency Modulated Manifolds in Dimensionality Reduction. Preprint 51, DFG-SPP 1324, June 2010.

[52] E. Herrholz and G. Teschke. Compressive Sensing Principles and Iterative Sparse Recovery for Inverse and Ill-Posed Problems. Preprint 52, DFG-SPP 1324, July 2010.

[53] L. Kämmerer, S. Kunis, and D. Potts. Interpolation Lattices for Hyperbolic Cross Trigonometric Polynomials. Preprint 53, DFG-SPP 1324, July 2010.

[54] G. Kutyniok and W.-Q Lim. Shearlets on Bounded Domains. Preprint 54, DFG-SPP 1324, July 2010.

[55] A. Zeiser. Wavelet Approximation in Weighted Sobolev Spaces of Mixed Order with Applications to the Electronic Schrödinger Equation. Preprint 55, DFG-SPP 1324, July 2010.

[56] G. Kutyniok, J. Lemvig, and W.-Q Lim. Compactly Supported Shearlets. Preprint 56, DFG-SPP 1324, July 2010.

[57] A. Zeiser. On the Optimality of the Inexact Inverse Iteration Coupled with Adaptive Finite Element Methods. Preprint 57, DFG-SPP 1324, July 2010.

[58] S. Jokar. Sparse Recovery and Kronecker Products. Preprint 58, DFG-SPP 1324, August 2010.

[59] T. Aboiyar, E. H. Georgoulis, and A. Iske. Adaptive ADER Methods Using Kernel-Based Polyharmonic Spline WENO Reconstruction. Preprint 59, DFG-SPP 1324, August 2010.

[60] O. G. Ernst, A. Mugler, H.-J. Starkloff, and E. Ullmann. On the Convergence of Generalized Polynomial Chaos Expansions. Preprint 60, DFG-SPP 1324, August 2010.

[61] S. Holtz, T. Rohwedder, and R. Schneider. On Manifolds of Tensors of Fixed TT-Rank. Preprint 61, DFG-SPP 1324, September 2010.

[62] J. Ballani, L. Grasedyck, and M. Kluge. Black Box Approximation of Tensors in Hierarchical Tucker Format. Preprint 62, DFG-SPP 1324, October 2010.

[63] M. Hansen. On Tensor Products of Quasi-Banach Spaces. Preprint 63, DFG-SPP 1324, October 2010.

[64] S. Dahlke, G. Steidl, and G. Teschke. Shearlet Coorbit Spaces: Compactly Supported Analyzing Shearlets, Traces and Embeddings. Preprint 64, DFG-SPP 1324, October 2010.

[65] W. Hackbusch. Tensorisation of Vectors and their Efficient Convolution. Preprint 65, DFG-SPP 1324, November 2010.

[66] P. A. Cioica, S. Dahlke, S. Kinzel, F. Lindner, T. Raasch, K. Ritter, and R. L. Schilling. Spatial Besov Regularity for Stochastic Partial Differential Equations on Lipschitz Domains. Preprint 66, DFG-SPP 1324, November 2010.

[67] E. Novak and H. Woźniakowski. On the Power of Function Values for the Approximation Problem in Various Settings. Preprint 67, DFG-SPP 1324, November 2010.

[68] A. Hinrichs, E. Novak, and H. Woźniakowski. The Curse of Dimensionality for Monotone and Convex Functions of Many Variables. Preprint 68, DFG-SPP 1324, November 2010.

[69] G. Kutyniok and W.-Q Lim. Image Separation Using Shearlets. Preprint 69, DFG-SPP 1324, November 2010.